Monthly Notices
of the
ROYAL ASTRONOMICAL SOCIETY

Mon. Not. R. Astron. Soc. **415,** 964–976 (2011) doi:10.1111/j.1365-2966.2011.18794.x

Future virialized structures: an analysis of superstructures in the SDSS-DR7

H. Luparello,[1⋆] M. Lares,[1] D. G. Lambas[1] and N. Padilla[2]

[1]*Instituto de Astronomía Teórica y Experimental (CONICET-UNC), Observatorio Astronómico de Córdoba, Laprida 854, X5000BGR, Córdoba, Argentina*
[2]*Departamento de Astronomía y Astrofísica, Pontificia Universidad Católica de Chile, Santiago, Chile*

Accepted 2011 March 24. Received 2011 March 22; in original form 2011 January 7

ABSTRACT

We construct catalogues of present superstructures that, according to a Λ cold dark matter (ΛCDM) scenario, will evolve into isolated, virialized structures in the future. We use a smoothed luminosity density map derived from galaxies in SDSS-DR7, Abazajian et al., data and separate high-luminosity density peaks. The luminosity density map is obtained from a volume-limited sample of galaxies in the spectroscopic galaxy catalogue, within the SDSS-DR7 footprint area and in the redshift range $0.04 < z < 0.12$. Other two samples are constructed for calibration and testing purposes, up to $z = 0.10$ and 0.15. The luminosity of each galaxy is spread using an Epanechnikov kernel of $8\,\mathrm{Mpc}\,h^{-1}$ radius, and the map is constructed on a $1\,\mathrm{Mpc}\,h^{-1}$ cubic cell grid. Future virialized structures (FVSs) are identified as regions with overdensity above a given threshold, calibrated using a ΛCDM numerical simulation and the criteria presented by Dünner et al. We assume a constant mass-to-luminosity ratio and impose the further condition of a minimum luminosity of $10^{12}\,\mathrm{L}_{\odot}$. According to our calibrations with a numerical simulation, these criteria lead to a negligible contamination by less overdense (non-FVS) superstructures. We present a catalogue of superstructures in the SDSS-DR7 area within redshift $0.04 < z < 0.12$ and test the reliability of our method by studying different subsamples as well as a mock catalogue. We compute the luminosity and volume distributions of the superstructures, finding that about 10 per cent of the luminosity (mass) will end up in future virialized structures. The fraction of groups and X-ray clusters in these superstructures is higher for groups/clusters of higher mass, suggesting that future cluster mergers will involve the most massive systems. We also analyse known structures in the present Universe and compare with our catalogue of FVSs.

Key words: methods: data analysis – methods: statistical – catalogues – large-scale structure of Universe.

1 INTRODUCTION

Structures in the universe are the result of a hierarchical process of accretion dominated, in almost all scales and during almost their entire history, by gravity. The first attempt to investigate the evidence for the existence of the so-called second-order clusters of galaxies was made by Shapley (1961), although there had been previous suggestions of the presence of large structures. Shapley & Ames (1930) suggested the presence of a large galaxy system in the Coma–Virgo region. Also, conglomerates composed by several clusters of galaxies observed in plates of the Lick Astrographic Survey were reported by Shane & Wirtanen (1954) and Shane (1956). By analysing the distribution of rich clusters identified on the National Geographic Society – Palomar Observatory Sky Survey, Abell pointed out that the clusters did not appear to be distributed randomly over the sky, but forming associations of matter on greater scales. Different authors adopted different methods to search for groups of clusters and the term supercluster became widely used. Abell used counts in cells to statistically test the distribution of clusters and endorsed the existence of superclusters of the order of $50\,h^{-1}$ Mpc in size. The first attempts to study superclusters on a statistical basis were made by linking Abell cluster positions (Zucca et al. 1993; Einasto et al. 1997). Later, the accomplishment of wide-area surveys of galaxies with spectroscopic follow-up, such as the Las Campanas Redshift Survey (Shectman et al. 1996), the 2-degree Field Galaxy Redshift Survey (2dFGRS, Colless et al. 2001) and the Sloan Digital Sky Survey (SDSS, Stoughton et al. 2002), allowed for the identification of superclusters directly from the large-scale galaxy distribution. Einasto et al. (2007b) identified superclusters in the 2dFGRS using a density field method, and recently Costa-Duarte, Sodré & Durret (2011) studied the morphology of superclusters of galaxies in the

⋆E-mail: heliana@mail.oac.uncor.edu

SDSS. The largest catalogue of superclusters has been constructed by Liivamägi, Tempel & Saar (2010) who implemented the density field method on the SDSS-DR7 main and luminous red galaxies (LRG) samples. In all cases, superclusters are operationally defined as objects within a region of positive galaxy density contrast and thus are subject to a certain degree of arbitrariness in the parameter selection.

Within the Λ cold dark matter (ΛCDM) concordance cosmological model, an accelerated expansion dominates the present and future dynamics of the universe and thus determines the nature of gravitationally bound structures. Therefore, an alternative definition of these large-scale structures may be derived from the properties of overdense regions in the present-day universe that will become bound and virialized structures in the future. Thus, under the assumption that luminosity is a somewhat unbiased tracer of mass on large scales, the integrated luminosity density of galaxies is commonly used as an indicator of mass density.

The cosmological evolution of the large-scale structure has implications on the spatial distribution, frequency and properties of superclusters and the galaxies they contain. Due to this relationship, superclusters can be used as cosmological probes, and their study is oriented to constrain models and describe the formation of superstructures on a cosmological scale. Supercluster properties have been used to discriminate between cosmological models, favouring the standard cosmological model in most cases (Basilakos, Plionis & Rowan-Robinson 2001; Peacock et al. 2001). On the other hand, there are claims of structures that are too massive or formed too early according to the standard model (Baugh et al. 2004).

First attempts to determine the characteristic scales of spatial inhomogeneities in the universe were made by Broadhurst et al. (1990) and Einasto et al. (1994). By studying the distribution of rich clusters of galaxies from the Abell-ACO catalogue, Einasto et al. (1994) confirmed a 110–140 h^{-1} Mpc scale in the supercluster–void network. Given the observed regular pattern of superclusters and voids, Frisch et al. (1995) investigated the properties of the initial power spectrum giving rise to these large-scale fluctuations. The authors found that the supercluster–supervoid network forms at a very early stage of the evolution of the Universe from large-scale density fluctuations and are defined by the scale of the maximum of the power spectrum.

The large-scale structure of the universe is often described as a supercluster–void network (Shandarin, Sheth & Sahni 2004), and superclusters are closely related to filaments (González & Padilla 2010; Murphy, Eke & Frenk 2011) and voids (Icke 1984; Einasto, Saar & Klypin 1986; Einasto et al. 1997; Park & Lee 2007; Platen, van de Weygaert & Jones 2008). Such filaments may also play an important role in the process of structure formation. Porter et al. (2008) find that star formation is significantly enhanced when galaxies fall into clusters along supercluster filaments. Superclusters have also been studied as hosts of Lyα absorbers (Stocke et al. 1995; Penton, Stocke & Shull 2002) and are known to produce signatures in the cosmic background radiation (Dolag et al. 2005; Génova-Santos et al. 2008; Flores-Cacho et al. 2009; Granett, Neyrinck & Szapudi 2009; Génova-Santos et al. 2010).

The aim of this work is to present and analyse catalogues of superstructures that will evolve into virialized systems. Using the theoretical framework of Dünner et al. (2006) in a ΛCDM scenario and by calibration with numerical simulations, we analyse volume-limited samples of galaxies from the SDSS-DR7.

This paper is organized as follows. In Section 2, we describe the data used in the computation of the density field. The methodological description of the procedures implemented to obtain the catalogue of future virialized structures (hereinafter FVSs) is addressed in Section 3, along with a brief description of the previous methodology employed in the search for superclusters. The catalogue of FVSs is presented in Section 4, where we also discuss some of their properties. In Section 5, we compare known superclusters with our identified structures and in Section 6 we study the frequency of clusters and groups of galaxies in FVSs. Our conclusions are summarized in Section 8. Throughout this paper, we adopt a concordance cosmological model ($\Omega_\Lambda = 0.75$, $\Omega_{\rm matter} = 0.25$) in the calculation of distances.

2 DATA AND SAMPLES

Since FVSs are extended regions of several tens of Mpc in size, a large volume of space has to be surveyed in order to sample a representative population of these objects. The SDSS (Stoughton et al. 2002) is the largest photometric and spectroscopic survey carried out so far, covering an area of almost a quarter of the sky with a limiting magnitude that makes the construction of complete samples of several hundred Mpc possible. Several catalogues have been made public by successive releases since the Early Data Release (Stoughton et al. 2002). The latest release of the spectroscopic catalogue (DR7, Abazajian et al. 2009) comprises 929 555 galaxy spectra within a footprint area of 9380 deg^2. The limiting apparent magnitude for the spectroscopic catalogue in the r band is 17.77 (Strauss et al. 2002), although we use a more conservative limit of 17.5 to ensure completeness. We also limit the sample to galaxies fainter than $r = 14.5$, since saturation effects in the photometric pipeline do not secure completeness below that limit. These limits were adopted taking into account the analysis of the image quality and efficiency detection of the SDSS.[1]

Given the dependence of the luminosity density field on the sample of galaxies, we define three complete samples, with different cuts in luminosity (Table 1). The closest sample comprises galaxies brighter than $M_r = -20.5$ up to $z = 0.1$. This is the sample with the faintest luminosity limit, and it will be mainly used to explore the effects of the luminosity cut in the detection of superstructures. This sample will be referred to as S1 and their characteristics are summarized in Table 1. A larger volume-limited sample, referred to as S3, contains all galaxies brighter than $M_r = -21.0$ to $z \leq 0.15$. An intermediate-redshift sample in the range $0.04 < z < 0.12$ comprises 89 513 galaxies. This sample, S2, containing galaxies with $M_r < -20.47$ will be analysed into detail in Sections 4–6.

In order to test procedures and results, we use the Millennium numerical simulation (Springel et al. 2005) of a ΛCDM concordance model, performed on a cubic box of 500 h^{-1} Mpc side. A semi-analytic model of galaxy formation (GALFORM, Bower, McCarthy & Benson 2008) collects information from the merger trees extracted from the simulation and generates a population of galaxies within the simulation box. We use the semi-analytic galaxy catalogue in the full box of the simulation to test and set the parameters involved in the identification of FVSs. We constructed a mock catalogue from the semi-analytic galaxies by following the geometry of the SDSS-DR7 footprint area and reproducing the dilution in the number of galaxies with redshift. In order to test the effect of peculiar velocities in the identification of FVSs, we defined a sample of galaxies in real,space, M_{Rsp}, and a sample of galaxies in redshift space, M_{Zsp}, also described in Table 1.

[1] http://www.sdss.org/dr7/products/general/target_quality.html

Table 1. Galaxy samples in the SDSS-DR7. In all cases $z \geq 0.04$ and the apparent magnitude in the r band is in the range $14.5 \leq r \leq 17.5$. The mean luminosity density, $\bar{\rho}_{\rm lum}$, is computed using volume-limited samples, each containing $N_{\rm gal}$ galaxies. The correction factor F (equation 6) and the resulting mean luminosity, $\bar{\rho}_{\rm lum}$, of each sample are indicated in the table.

Sample	$z_{\rm max}$	$D_{\rm max}$ (h^{-1} Mpc)	$M_r^{\rm lim}$	Volume [$10^7(h^{-1}$ Mpc$)^3$]	$N_{\rm gal}$	$\bar{\rho}_{\rm lum}(10^8\,{\rm L}_\odot\,{\rm Mpc}^{-3})$	F	Corrected $\bar{\rho}_{\rm lum}(10^8\,{\rm L}_\odot\,{\rm Mpc}^{-3})$
S1	0.10	293.92	−20.05	1.85	94 271	0.80	2.11	1.68
S2	0.12	351.34	−20.47	3.17	89 513	0.58	2.98	1.73
S3	0.15	436.55	−21.00	6.01	62 344	0.29	5.66	1.64
S2c	0.10	293.92	−20.47	1.85	51 188	0.56	2.98	1.73
S3c	0.10	293.92	−21.00	1.85	17 507	0.27	5.66	1.64
M_{Rsp}	0.12	351.34	−20.47	3.17	106 604	0.75	2.98	2.23
M_{Zsp}	0.12	351.34	−20.47	3.17	106 722	0.75	2.98	2.23

We use AB magnitudes and apply k+e corrections in the rest frame at $z = 0.1$, as defined in Blanton et al. (2003a). From these magnitudes, we calculate the luminosity of each galaxy, in the r band, as $L = 10^{0.4({\rm M}_\odot - M_r)}{\rm L}_\odot$. The mean luminosity density $\bar{\rho}_{\rm lum}$ of each sample is computed with this luminosity and is also listed in Table 1. We will also study the properties of groups and clusters of galaxies within FVSs. To this end, we use a catalogue of galaxy groups in the SDSS-DR7 compiled by Zapata et al. (2009). This catalogue is obtained using an adaptative Friends-of-Friends method. Virial masses are computed from the line-of-sight velocity dispersion of galaxies in each group ($\sigma_{\rm v}$) and the virial radius ($R_{\rm vir}$), using the virial theorem (see Zapata et al. 2009):

$$M_{\rm vir} = \frac{3\sigma_{\rm v}^2 R_{\rm vir}}{G}, \quad (1)$$

where $R_{\rm vir}$ is estimated as in Merchán & Zandivarez (2005). The catalogue comprises 83 784 groups with at least four members and is limited to redshift $z < 0.12$.

We have also analysed a catalogue of X-ray-selected clusters (Popesso et al. 2004) in order to study the presence of large gravitational potential wells in FVSs. This sample comprises 114 clusters with X-ray emission and is based on the ROSAT All Sky Survey (RASS) and the SDSS. The total luminosity in the *ROSAT* band is available for each cluster and is used as a proxy for the cluster mass (Rykoff et al. 2008). We use this luminosity in Section 6 to explore the variations with X-ray luminosity of the fraction of clusters belonging to FVSs.

3 METHOD

3.1 Previous analyses

Several procedures have been proposed to construct a reliable catalogue of superstructures, although they are based on different criteria and methods. The main issue related to the comparison of superstructure catalogues is that the definition of superstructures depends on the specific choice of a number of free parameters. Einasto et al. (1997) use a percolation algorithm to link clusters of galaxies from the Abell-ACO catalogue and derive a catalogue of 220 superclusters of rich clusters within $z = 0.12$. The authors percolate clusters lying within a given radius from each other, defining these systems of clusters as superclusters. They find that a percolation radius of $24\,h^{-1}$ Mpc is convenient to detect the largest, but still relatively isolated, systems of clusters. The main results from the supercluster catalogue are not, according to the authors, very sensitive to the exact value of the percolation radius. Einasto et al. (2001) updated the catalogue with a newer version of the Abell catalogue, incorporating in the analysis a sample of X-ray clusters; this also allowed them to compare superclusters derived from different samples of clusters. They find that both types of clusters generate superstructures that represent the large-scale structure in a similar way. Also, they find that X-ray clusters not belonging to superclusters surround the Southern and Northern Local supervoids or are located in filaments between superclusters. Although the authors find a strong signal indicating that the fraction of X-ray clusters in superclusters increases with supercluster richness, there is no correlation between the X-ray luminosity of clusters and their host supercluster richness, quantified as the number of member clusters. Einasto et al. (2007b) return to the problem of defining the largest isolated structures in the universe and use data from the 2dFGRS (Colless et al. 2001) to assemble a catalogue of superclusters. The authors find that the most effective method to perform a supercluster search is the density field method which consists in obtaining a smoothed luminosity density field in redshift space from the galaxy catalogue. The luminosity, on large scales, is supposed to follow the distribution of matter, provided that a convenient smoothing kernel is used. In their work, Einasto et al. (2007b) use an Epanechnikov kernel and assert that the best results in the identification method are obtained when a kernel size of $8\,h^{-1}$ Mpc is used. Einasto et al. (2007b) set the threshold parameter by maximizing the number of large superclusters. Costa-Duarte et al. (2011) apply the density field method to the SDSS-DR7 and use two samples of structures, selected using different overdensity thresholds. The authors claim that there is no natural value for the threshold density and define a sample that maximizes the number of structures, and a sample with the parameters tuned so that the largest superclusters present an extension of $\approx 120\,h^{-1}$ Mpc. The authors perform an analysis of the shapes of superclusters using Minkowski functionals, finding that filamentary structures tend to be richer, larger and more luminous than pancakes. They also use a semi-analytic catalogue of galaxies derived from the Millennium simulation to test the method and conclude that the morphological classification is not biased by peculiar velocities. Liivamägi et al. (2010) use a similar approach, but perform the smoothing with a B3-spline kernel of radius of $8\,h^{-1}$ Mpc, obtaining catalogues of superstructures with similar properties in the SDSS-DR7 and in the Millennium simulation.

3.2 Present approach

Given that not all large-scale structures are virialized at the present time, the setting of identification parameters is subject to certain degree of arbitrariness. A physically motivated threshold on mass overdensity was explored in ΛCDM simulations by Dünner et al. (2006). According to these authors, it is possible to define a criterion to isolate, using three-dimensional data, overdensity regions

enclosed by a spherical shell that will evolve into virialized systems. By the application of the spherical collapse model, the mean mass density enclosed by the last bound shell of a structure must satisfy

$$\frac{\bar{\rho}^{\rm mass}_{\rm shell}}{\bar{\rho}^{\rm mass}_{\rm bck}} = 7.88, \tag{2}$$

where $\bar{\rho}^{\rm mass}_{\rm shell}$ is the mean mass density enclosed by the critical shell (the shell that maximizes the potential energy) and $\bar{\rho}^{\rm mass}_{\rm bck}$ is the mean density of the background. In observational catalogues, there is not an accurate estimation of the mass density field. However, given that at large scales the mass-to-luminosity ratio is nearly constant, we can apply a similar criterion to the luminosity map to derive structures with an appropriate mass overdensity.

In the following subsections, we describe the identification method implemented on the SDSS-DR7 spectroscopic data. We first define the volume covered by the sample using a three-dimensional mask and construct a luminosity density map with a $1\,(h^{-1}\,{\rm Mpc})^3$ cell resolution. We then use a percolation method based on the search of high-density peaks on the three-dimensional smoothed map. These overdensities are the basis of the superstructure catalogue.

3.2.1 *Luminosity density map*

We construct smooth luminosity density maps from our complete samples of galaxies, in the region defined by a three-dimensional mask. This mask, which represents an approximation of the geometry of the SDSS-DR7 galaxy catalogue in both angular coordinates and redshift, is built using cubic cells of $1\,h^{-1}$ Mpc side. We start from a pixelized representation of the central region within the catalogue footprint area. To this end, we use an angular mask obtained using the software HEALPIX (Górski et al. 2005) with a resolution parameter $N_{\rm side} = 512$ that splits the whole sphere in 3145 728 equal-area pixels. A cubic cell is part of the three-dimensional mask if at least a fraction of its area includes part of the solid angle subtended by the angular mask, and its radial position lies within the redshift range defined for a given sample. We define the volume of a cell within the three-dimensional mask as $V'_{\rm cell} = V \times f_{\rm cell}$, where $V = (1\,h^{-1}\,{\rm Mpc})^3$ and $f_{\rm cell}$ measures the fraction of the volume V into the mask. We compute the fraction $f_{\rm cell}$ by implementing a Monte Carlo procedure. Accordingly, cells that are completely contained within the geometry of the catalogue have $f_{\rm cell} = 1$, while external cells have $f_{\rm cell} = 0$. The factor $f_{\rm cell}$ allows us to correct for border effects; in our subsequent analysis, we will use only cells with $f_{\rm cell} > 0.5$, that is, only cells with at least 50 per cent of their volume inside the mask. The continuous luminosity density map can be constructed by smoothing the galaxy distribution within the three-dimensional mask. A standard procedure to accomplish this consists in using a kernel function to convolve the discrete positions of galaxies and spread their luminosity. The resulting density field is then represented at a resolution given by the cell size and corrected by the weight factor $f_{\rm cell}$. The result of the smoothing depends on the shape and size of the chosen kernel function. Following previous analyses in the literature (Einasto et al. 2007c; Costa-Duarte et al. 2011), we use an Epanechnikov kernel of $r_0 = 8\,h^{-1}$ Mpc size, which gives the contribution at position $\boldsymbol{r}$ from a source that is located at $\boldsymbol{R}$:

$$k(\boldsymbol{r} - \boldsymbol{R}) = \frac{3}{4r_0}\left[1 - \left(\frac{|\boldsymbol{r} - \boldsymbol{R}|}{r_0}\right)^2\right]. \tag{3}$$

An Epanechnikov kernel is more suitable for this analysis since its shape resembles that of a Gaussian, but it avoids excessive smoothing. The luminosity density estimate within a cell is then

$$\rho_{\rm cell} = \frac{L_{\rm cell}}{V'_{\rm cell}}, \tag{4}$$

where $V'_{\rm cell} = V \times f_{\rm cell}$ is the volume of the cell and $L_{\rm cell}$ is the sum of the contributions to the luminosity $L_{\rm glx}$ from nearby galaxies:

$$L_{\rm cell} = \sum_i L^i_{\rm glx} \int_{\rm cell} k(\boldsymbol{r} - \boldsymbol{R}_i)\,{\rm d}\boldsymbol{r}. \tag{5}$$

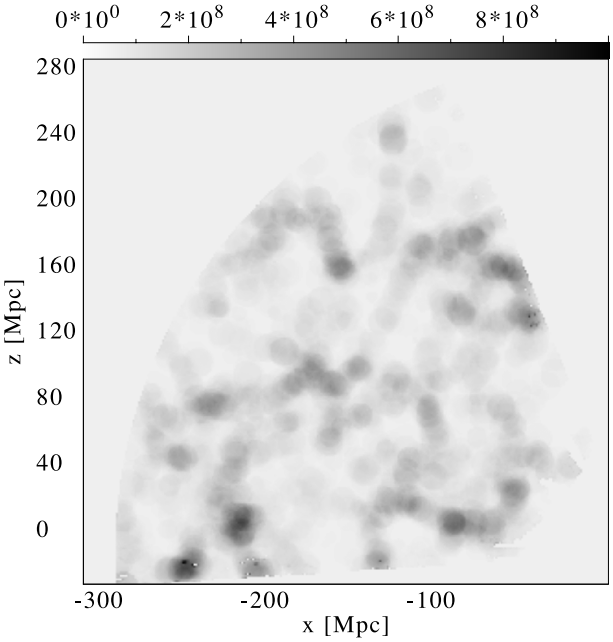

Figure 1. A slice of the luminosity density map for sample S2. The Cartesian system used is associated with the equatorial coordinate system, with the z-axis towards the north celestial pole. The smoothing kernel has an Epanechnikov shape, with a size of $8\,h^{-1}$ Mpc.

A slice of the map is shown in Fig. 1, where the large-scale structure of the luminosity distribution can be appreciated. Concentrations of galaxies such as rich groups or clusters are characterized by luminosity density peaks and are surrounded by low-density regions.

3.3 Identification of structures

We search for large isolated regions above a given density threshold; these are candidates to FVSs. The luminosity density, however, depends on the limiting magnitude characterizing a given volume-limited sample, which determines the number and luminosity of galaxies contributing to the overall density estimate. For example, deeper volume-limited samples include only brighter galaxies; thus, the luminosities of the cells will be systematically lower as the upper redshift limit of the sample increases. We use the luminosity overdensity instead of the total luminosity density value to characterize the peaks in the luminosity distribution, but still, since we study three samples with different limiting redshifts, a correction factor must be implemented in order to make the results as comparable as possible. This factor can be obtained by assuming a universal luminosity function for galaxies $\Phi(L)$, which allows us to account for the luminosity below the limiting value characterizing a given sample. Since the underestimation of the total luminosity depends only on the absolute magnitude cut $M_{\rm lim}$ of the sample, an homogeneous correction factor F for the entire luminosity density map can

be defined as

$$F = \frac{\int_0^\infty L\Phi(L)\,\mathrm{d}L}{\int_{M_{\rm lim}}^\infty L\Phi(L)\,\mathrm{d}L}. \quad (6)$$

We adopted the luminosity function presented by Blanton et al. (2003b). This correction ranges from 2 to $\lesssim$6 for samples with limiting absolute magnitudes down to $M_r = -21$. In Table 1, the correction factor F and the corrected mean luminosity density are listed for each sample.

We define superstructures by linking overdense cells using a Friends-of-Friends algorithm that connects overdense cells sharing at least one common vertex or side. To this end, we use the threshold luminosity overdensity criterion $\rho_{\rm lum\text{-}cell} \geq D_{\rm T}\,\bar{\rho}_{\rm lum}$. Since the properties of the catalogue of superstructures may be affected by the adopted value of the luminosity overdensity parameter $D_{\rm T}$, it is fundamental to study this issue in further detail.

3.4 Calibrating the method with numerical simulations

We use numerical simulations to test the ability of a luminosity-based algorithm to derive structures that will evolve into virialized systems in the future. We have also used the simulations to analyse whether superstructures identified in redshift space with total luminosities above $L = 10^{12}\,\mathrm{L}_\odot$ correspond to systems in real space above this threshold. This is an important issue to be checked since the observations provide redshift-space data, whereas the FVS criterion requires real-space information. In Fig. 2, we show the distributions of mass overdensity (only known in the simulations) for the sample of structures that result from the identification algorithm for

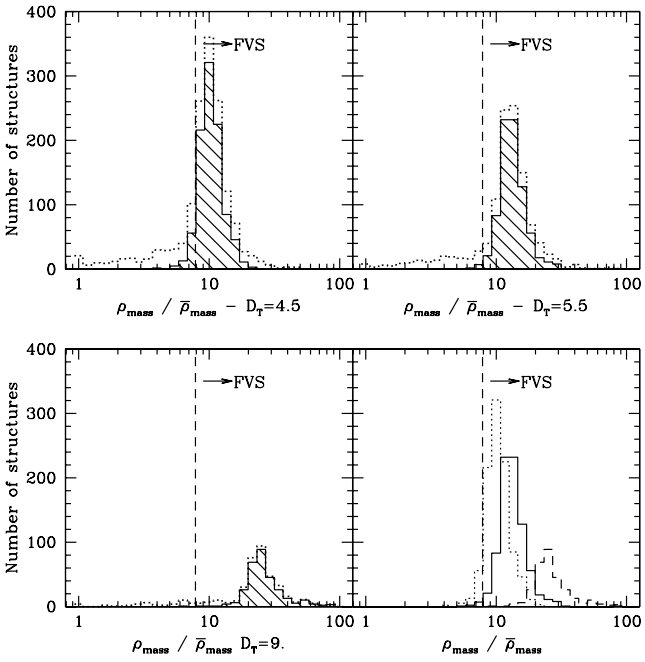

Figure 2. Distribution of the mass overdensity of the superstructures identified in the simulation box, for different values of the luminosity overdensity parameter ($D_{\rm T} = 4.5$, 5.5 and 9, in the top left-hand, top right-hand and bottom left-hand panels, respectively). The dashed vertical lines indicate the critical mass overdensity that a region must have to be virialized, according to Dünner et al. (2006). The dotted histograms show the distributions for the total sample of superstructures and black continuous histograms show the corresponding distributions for structures with the total luminosity greater than $10^{12}\,\mathrm{L}_\odot$. Bottom right-hand panel: comparison between the distributions of mass overdensity for the three values of $D_{\rm T}$.

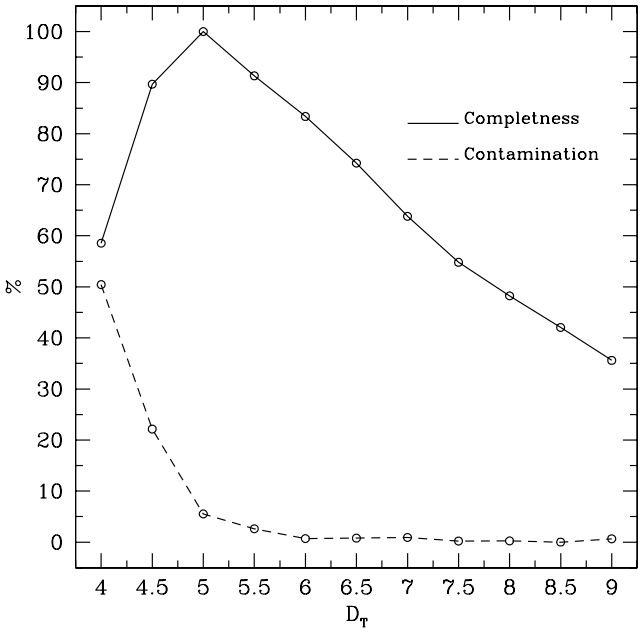

Figure 3. Completeness and contamination of the FVS catalogue as a function of $D_{\rm T}$. The chosen value of $D_{\rm T} = 5.5$ for the compilation of the catalogue of FVSs shows the best balance between low contamination and high completeness.

three different values of $D_{\rm T}$ and the corresponding distributions for superstructures with a luminosity above the threshold $10^{12}\,\mathrm{L}_\odot$. This adopted luminosity threshold is approximately the maximum observed value for a rich cluster of galaxies; by imposing this luminosity cut-off, we exclude individual clusters from our FVS catalogue. The bottom right-hand panel of Fig. 2 shows the mass overdensity of superstructures with the luminosity cut-off for three values in the luminosity overdensity parameter. The vertical dashed line in this figure shows the minimum mass overdensity for a superstructure to be virialized in the future according to Dünner et al. (2006). As can be seen, the contamination in the catalogue depends on the choice of the luminosity overdensity parameter. In order to select the most convenient value of this parameter, we explored the contamination and completeness of superstructures for different values of $D_{\rm T}$. We define the completeness as the ratio of the number of superstructures resulting from a given value of $D_{\rm T}$ and maximum number of superstructures obtained within the explored $D_{\rm T}$ range. Similarly, the contamination is defined as the fraction of identified superstructures that do not satisfy the future virialized criteria. In Fig. 3, we show the completeness and contamination parameters for the range $4 < D_{\rm T} < 9$. By inspection of this figure, we chose a luminosity overdensity threshold $D_{\rm T} = 5.5$. This adopted value provides a suitable compromise of high completeness and low contamination.

3.5 Redshift-space versus real-space analysis

In this subsection, we analyse the effects of redshift-space distortions induced by peculiar velocities on the identification of FVSs, using the mock catalogue. We considered the mock catalogue to construct samples of galaxies in redshift-space (M_{Zsp}) and in real-space (M_{Rsp}), defined using the same redshift limits and limiting absolute magnitudes as sample S2 (see Table 1). This allows to study FVSs identified in real space and compare them with those selected in redshift space. We have computed the distributions of the luminosity and volume derived for the FVS in these mock samples.

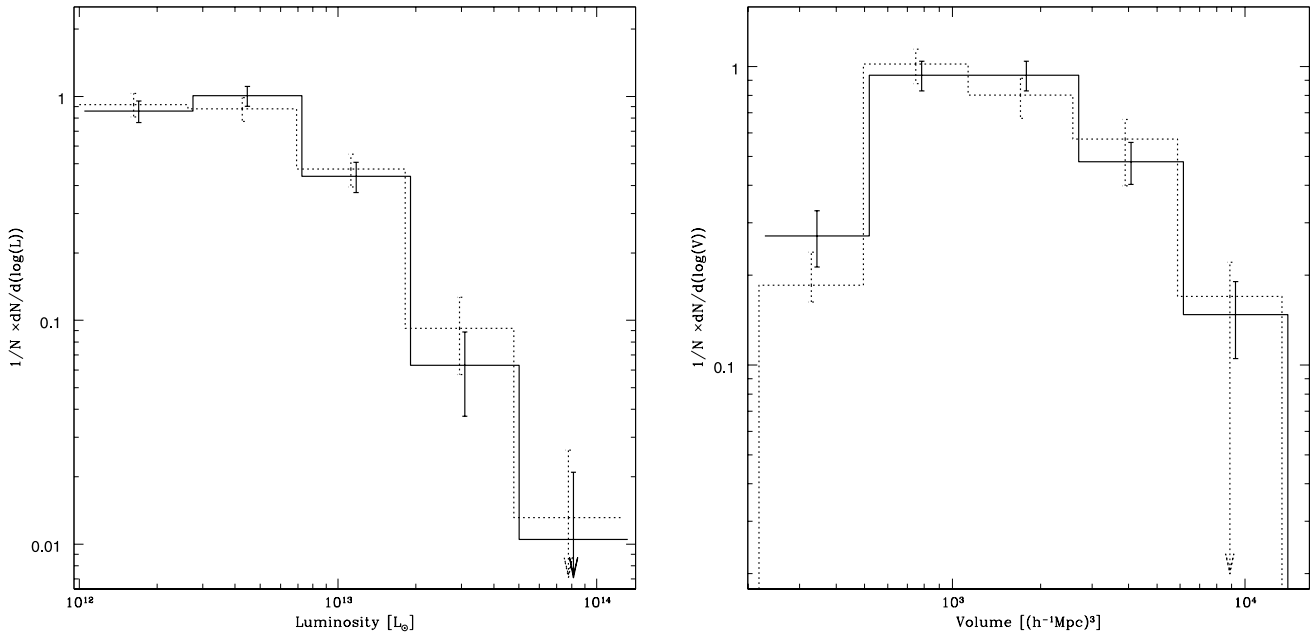

Figure 4. Histograms representing the luminosity (a) and volume (b) distributions of FVSs. The solid lines correspond to the sample of FVSs identified in sample M_{Zsp} (redshift-space mock, see Section 2) and the dotted lines correspond to FVSs identified in sample M_{Rsp} (real-space mock).

A good agreement can be appreciated between the luminosity distributions (Fig. 4a), indicating that the identification procedure delivers reliable estimations of the total luminosity. It can also be inferred from the volume distributions, shown in Fig. 4(b), that the volume of FVSs is not strongly affected by peculiar velocities.

We also analysed the correspondence between structures in real and redshift space in order to estimate the contamination and completeness of the FVS catalogue. The first point we note is the lower number of FVSs identified in the redshift-space sample compared to that of the real-space sample, in the same volume. About 20 per cent of FVSs identified in real space are lost when analysing redshift-space data. This is a major drawback of redshift-space FVS identification. On the other hand, only 2 per cent of FVSs identified in redshift space are not real-space FVSs. This indicates that the identification of FVSs in observational catalogues is not likely to include fake FVS structures. We also found that approximately 3 per cent of FVSs in the mock catalogue are associated with more than a single FVS in real space. A similar percentage of real-space FVSs are identified as multiple FVSs in redshift space.

4 CATALOGUE OF FVSs

Taking into account the results of the previous sections, we have adopted a luminosity overdensity threshold of $D_T = 5.5$ and in order to avoid the inclusion of spurious systems, a lower luminosity limit $L_{str} > 10^{12}\,L_\odot$. In Table 2, we summarize some characteristics of the identified FVS.

Once the superstructures have been identified, it is important to assess their fundamental properties such as the total volume, the number of galaxies above a given luminosity, the total luminosity, shape parameters, etc. Given the small volume of sample S1, and the large luminosity correction factor in sample S3, we provide an analysis of sample S2 in what follows.

Table 2. Main results obtained for the samples of identified FVSs. For each sample, we show the number of FVSs, N_{FVS}, the percentage of volume occupied by FVSs, F_{vol}, the percentage of the luminosity of galaxies within FVSs, F_{lum}, and the total number of galaxies within FVSs, $glxs_{in\,FVS}$.

Sample	N_{FVS}	F_{vol}	F_{lum}	$glxs_{in\,FVS}$
S1	67	1.08 per cent	10.85 per cent	9707
S2	150	1.26 per cent	13.54 per cent	11 394
S3	412	1.66 per cent	20.61 per cent	11 682
M_{Rsp}	227	1.62 per cent	18.87 per cent	19 265
M_{Zsp}	181	1.35 per cent	15.14 per cent	15 368

4.1 Analysis of the FVS catalogue (sample S2)

In Fig. 5(a), we show the distribution of luminosities of the superstructures we obtain for the SDSS-DR7. FVS luminosities vary between 10^{12} and $\sim 10^{14}\,L_\odot$, in agreement with Einasto et al. (2006) and Costa-Duarte et al. (2011). However, Einasto et al. (2006) find a lack of luminous superclusters in numerical simulations compared to superclusters identified in observational catalogues. In a forthcoming paper (Luparello et al., in preparation), we will analyse this issue in more detail.

Since the superstructures are obtained from a discrete density map, the volume can be directly calculated as the sum of the volumes of all the cells that belong to a given system. As all cells have the same volume, equal to 1 $(h^{-1}\,\mathrm{Mpc})^3$, the number of cells that form a structure is directly proportional to the volume. As it can be appreciated in Fig. 5(b), the volume of the superstructures ranges between 10^2 and $10^5 (h^{-1}\,\mathrm{Mpc})^3$. We also compute the fraction of the total volume that is in FVSs, finding that FVSs represent only 1.26 per cent of the volume covered by sample S2. Einasto et al. (2007a) found that the volume covered by superclusters in the 2dFGRS represents 3.2 per cent of the Northern region of the catalogue and 3.5 per cent of the Southern region. Our lower percentages

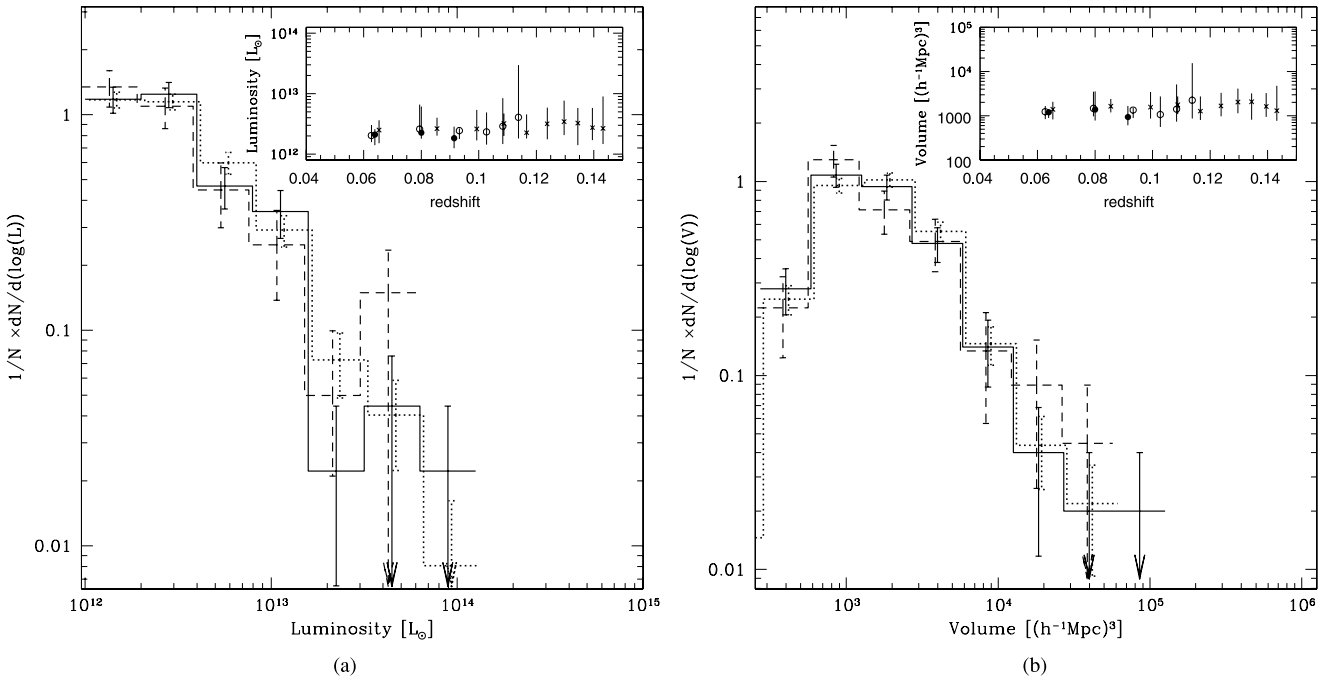

Figure 5. Luminosity (a) and volume (b) distributions of structures for samples S1 (dashed line), S2 (solid line) and S3 (dotted line). The insets show the average volume and luminosity as a function of the redshift, in redshift bins with equal numbers of superstructures, with the filled circles, empty circles and cruxes, respectively, for samples S1, S2 and S3. Error bars on the histograms indicate Poisson uncertainty. In the inset box, the uncertainty bars correspond to the 25 and 75 per cent percentiles.

can be explained by the fact that we use a higher value of $D_{\rm T}$ and impose a limit of at least $10^{12}\,{\rm L}_{\odot}$ in the luminosity of the superstructures.

Previous analyses of numerical simulations have shown that the shapes of haloes are consistent with an increasing elongation as the mass increases. This is also detected in observational data (Paz et al. 2006), where the most massive structures tend to be prolate. We note that the shapes of FVSs are somewhat irregular since several of these systems are composed of a few filaments or pancakes of irregular shapes, joined by one or two vertices. Nevertheless, in order to provide a rough characterization of FVS shapes, we use the usually adopted ellipsoidal model to study the distribution of axial ratios. We have computed the moment of inertia $I_{ij} = \sum_{\rm gxs}(x_i^{\rm gx} - C_i^{\rm FVS})(x_j^{\rm gx} - C_j^{\rm FVS})$, where $x_i^{\rm gx}$ is the ith coordinate (i.e. the x-, y- or z-axis) of the member galaxies and $C_i^{\rm FVS}$ are the coordinates of the geometrical centre of each FVS. The diagonalization of this matrix gives the values of the three axes of the ellipsoid with the same moment of inertia, a, b and c. In the inset of Fig. 6, we show the results of the axial ratios of FVSs in a c/b versus b/a diagram. As can be seen from this figure, neither spherical ($a \sim b \sim c$) nor planar ($b \sim a > c$) structures are common; there is a preference for prolate-shaped FVS structures. We use the triaxiality parameter $T = [1 - (b/a)^2]/[1 - (c/a)^2]$ adopted by Wray et al. (2006) who analysed supercluster shapes in a ΛCDM model simulation. This parameter takes values between 0 and 1; $T \sim 0$ indicates oblate structures, while $T \sim 1$ indicates prolate structures. Intermediate values of T represent triaxial systems, with triaxiality increasing (not linearly) with T. We show in Fig. 6 the distribution of T for samples S2, M_{Zsp} and M_{Rsp}. As it can be seen from this figure, the distribution of shapes is not strongly affected by peculiar velocities. Also, it can be appreciated that the observed SDSS FVS shapes are consistent with those of ΛCDM structures. The mean value of this parameter is $T = 0.75 \pm 0.23$ for the main sample of FVSs of the SDSS and $T = 0.77 \pm 0.23$ for the sample of the real-space simulated catalogue. This indicates that these structures are mainly triaxial systems, and the distribution of T shows the predominance of prolate systems over oblate systems, in agreement with Einasto et al. (2007a). The

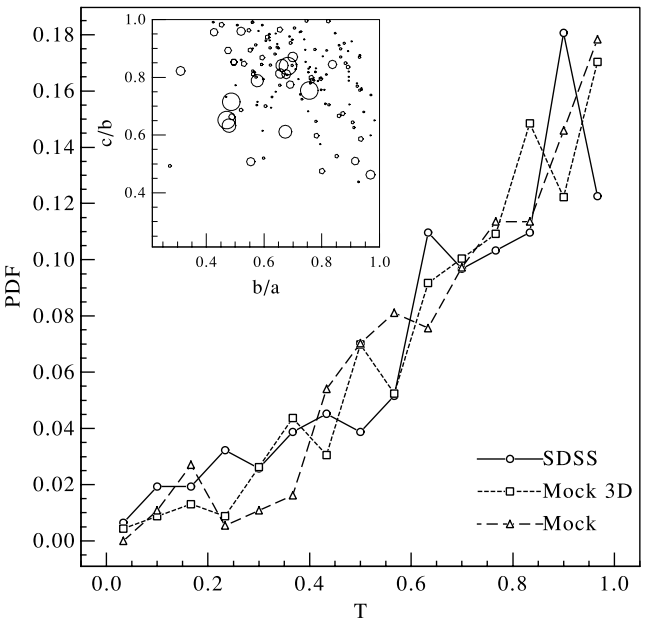

Figure 6. Probability density distribution estimates of the shape indicator parameter T (defined in Section 4.1). The distributions correspond to FVSs from the SDSS galaxy catalogue (solid line), the real-space mock catalogue (short-dashed line) and the redshift-space mock catalogue (long-dashed line). The inset shows a scatter plot of the semi-axial ratios c/b and b/a that characterize the shapes of the FVS. The sizes of the circles are proportional to the number of galaxies contained in each FVS.

mean values of T reported by Wray et al. (2006) range between $T = 0.65$ and 0.69, depending on the linking length, in agreement with our results. Costa-Duarte et al. (2011) present evidence of a trend between supercluster luminosities and shapes, where filaments are on average more luminous than pancakes. We also explored the dependence of the T parameter on FVS luminosity and volume, finding a similar tendency. Larger values of T correspond to more luminous, larger, FVSs.

4.2 Testing the reliability of the method

4.2.1 Redshift dependence

We have also searched for a possible redshift dependence of our results; note that, given the shallow depth of our samples, this constitutes a test of our method rather than a search for true time evolution. To this aim, we use samples S1 and S3, defined in Section 2. The similarity of the three histograms in Figs 5(a) and (b) corresponding to these different subsamples shows a lack of redshift dependence. This is also seen in the insets of Figs 5(a) and (b). As it can be seen, there is no significant dependence of the median luminosities and volumes on redshift, indicating the reliability of the method and its lack of a redshift bias.

4.2.2 Luminosity cut-off dependence

With the aim of analysing the effects of using tracers of different luminosities, we applied three magnitude cuts, corresponding to those of samples S2 and S3, to galaxies in the redshift range $0.04 \leq z \leq 0.10$. This defines two new samples: S2c and S3c, as described in Table 1. In Figs 7(a) and (b), we show the distribution of luminosities and volumes of FVSs selected from samples S1, S2c and S3c. We recall that we have applied the corresponding completeness luminosity factor F (equation 6) to the luminosities of FVSs. As can be seen from these figures, there is a very good agreement between the FVSs derived from these different galaxy tracers. These tests give confidence that the use of volume-limited samples of high-luminosity galaxies does not significantly change the results, with the advantage that they can trace larger volumes.

5 CORRESPONDENCE OF KNOWN SUPERCLUSTERS AND FVSs

As mentioned in Section 3, superclusters have been previously identified either as luminosity density enhancements or as systems of galaxy clusters. None of the criteria ensures that the structures will evolve into gravitationally virialized structures.

Therefore, it cannot be ensured that all known superclusters will be 'island universes' in the future. Recent supercluster catalogues were compiled from the 2dFGRS (Einasto et al. 2007b), SDSS-DR4 (Einasto et al. 2006) and SDSS-DR7 (Costa-Duarte et al. 2011). Since some of these catalogues cover only partially the volume of the central zone of the SDSS-DR7, we also used the supercluster identification of Einasto et al. (2001), where the identification is based on X-ray-selected and Abell clusters. Combining data from these catalogues, we can correlate our results with previous identifications and explore which known superclusters will also be FVSs, at least within the ΛCDM scenario. In Fig. 8, we show the FVS associated with the Sloan Great Wall, Ursa Major, Corona Borealis and Bootes superclusters. This figure shows the galaxies belonging to FVSs associated with each of the above-mentioned superclusters and also the galaxies in neighbouring FVSs. For comparison, the locations of the centres of superclusters in the same region, obtained from the literature, are presented.

Sloan Great Wall. There are several identified structures in the region associated with the Sloan Great Wall. Einasto et al. (2001) claim that the structures in their catalogue named SCL111 (a.k.a. Virgo–Coma) and SCL126 are part of the Sloan Great Wall. Of these superclusters, SCL126 is the richest in the Sloan Great Wall.

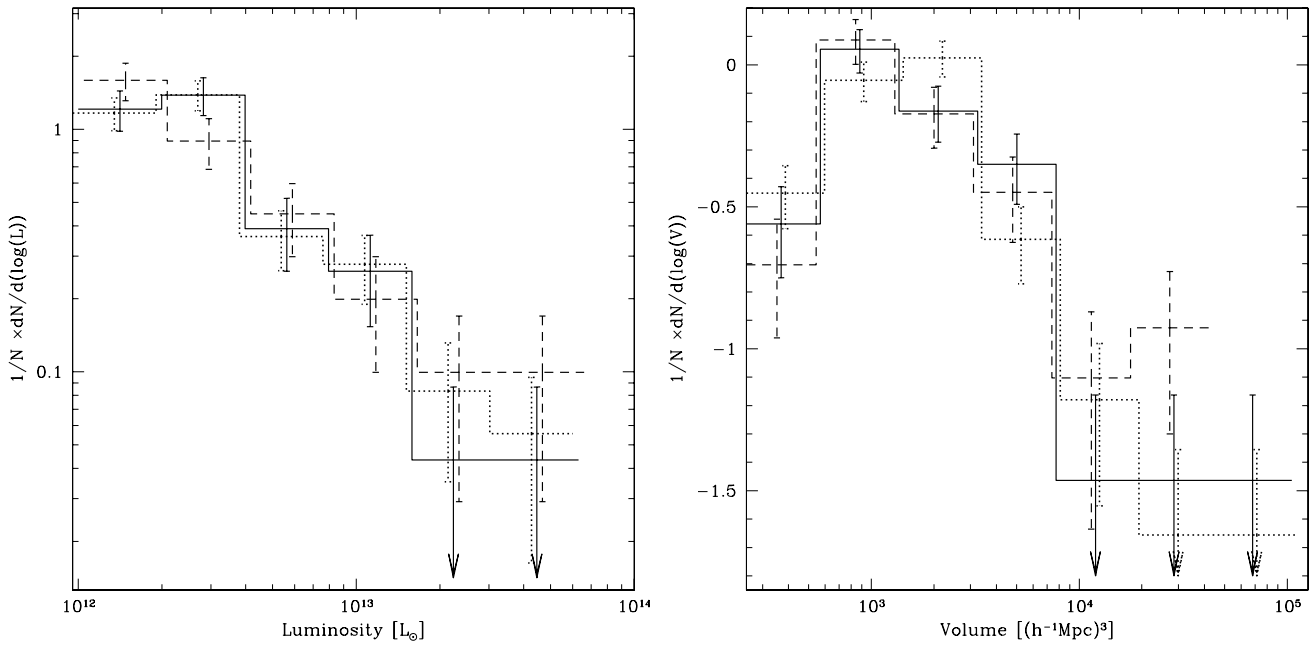

Figure 7. Luminosity (a) and volume (b) distributions of structures for samples S1 (dashed line), S2c (solid line) and S3c (dotted line). These three samples are limited to $z \leq 0.1$, but comprise galaxies with different absolute limiting magnitudes (see Table 1). Error bars are Poisson uncertainties within each bin.

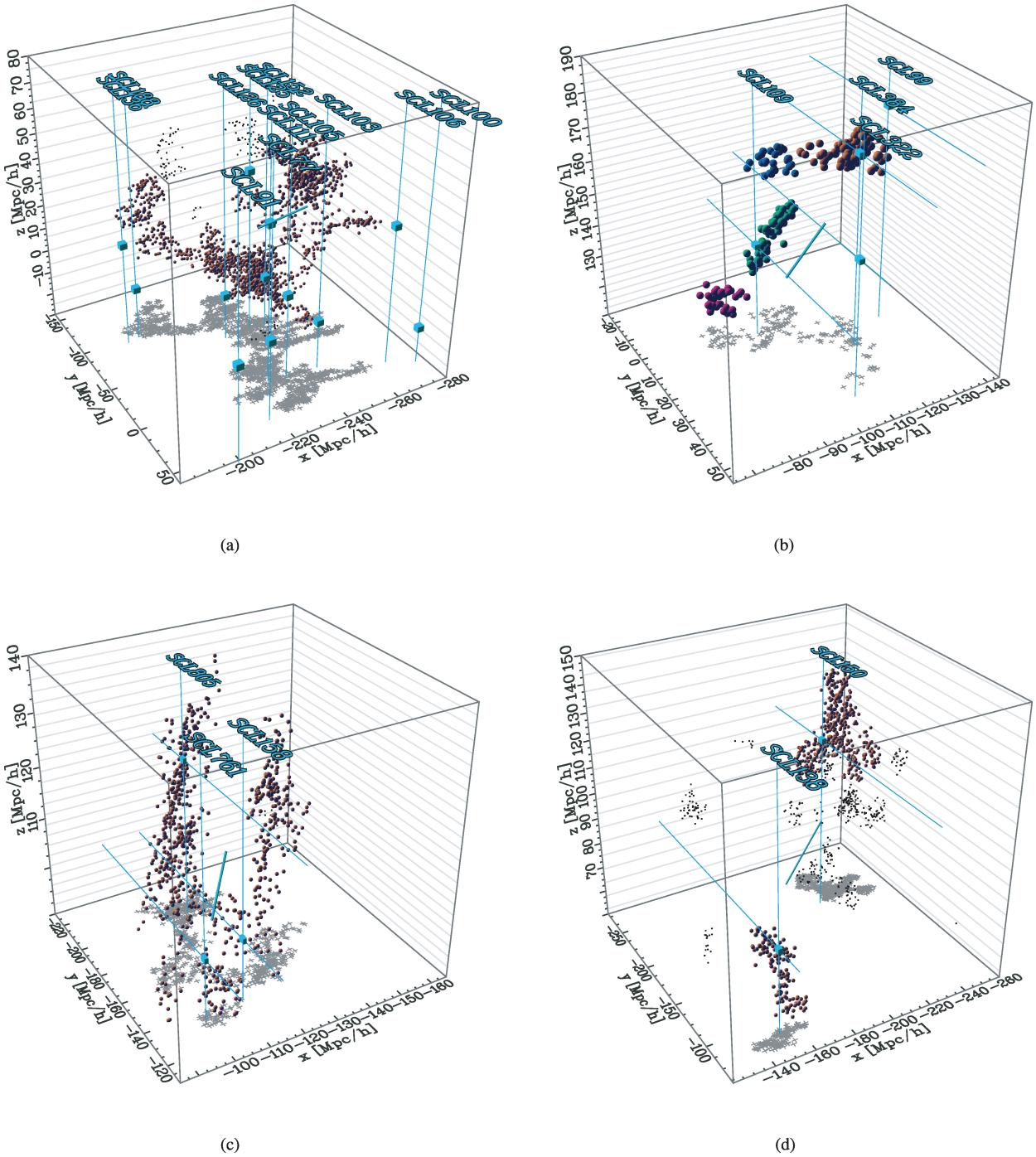

Figure 8. Spatial distributions of galaxies within FVSs associated with known superclusters (filled circles). The positions are shown in a Cartesian system associated with the equatorial coordinate system (x-axis pointing to the vernal point γ and z-axis pointing to the north equatorial pole); the line indicates the observer direction. We also show the centres of superclusters in the catalogues of Einasto et al. (2001), Einasto et al. (2007b) and Einasto et al. (2006). Galaxies within nearby FVSs are indicated with the black dots. In the Sloan Great Wall region (a), we identify a single FVS associated with SCL111, SCL126 and SCL136, indicating that these superclusters may evolve into a single virialized system. The Ursa Major supercluster, in (b), consists of three large filaments (Kopylova & Kopylov 2006). However, we find a different FVS associated with each filament, suggesting that the filaments would evolve into separate structures. In (c), the Corona Borealis supercluster SCL158 is part of a larger FVS that also includes SCL805 and SCL761. So, these three systems could merge to form a single virialized structure in the future. The Bootes and BootesA superclusters in (d) have one-to-one correspondence with FVSs, so each system would evolve into a FVS.

Einasto et al. (2010a) find that the structure previously identified as SCL136 in Einasto et al. (2001) is in fact a part of SCL126, and SCL111 comprises three concentrations of rich clusters connected by filaments of galaxies. Einasto et al. (2010a) also find the presence of substructures, indicating possible mergers and infall in different superclusters belonging to the Sloan Great Wall region, suggesting that the cores of these superclusters are not virialized and still assembling. We find that, according to the catalogue of FVSs, SCL111

and SCL126 may evolve into a single virialized structure, while the neighbouring SCL91 could remain isolated. The structure SCL100 (Einasto et al. 2001), associated with the Leo A supercluster and located near the Sloan Great Wall, has no FVSs that it can be directly associated with. We find several FVSs surrounding the centre of SCL100, thus suggesting that this supercluster could be disrupted in the future.

Ursa Major supercluster. Ursa Major is a nearby $z \simeq 0.06$ and relatively isolated supercluster. It has been found to be composed of three large filaments with the mean redshifts $z = 0.051$, 0.060 and 0.071 (Kopylova & Kopylov 2006). Einasto et al. (2001) associate Ursa Major to the SLC109 superstructure in their catalogue and present its geometrical centre located at $\alpha = 177.^{\circ}1$, $\delta = +55.^{\circ}0$ and $z = 0.06$. Einasto et al. (2006) identified the more distant filament as another individual supercluster (SCL384). We found four different FVSs with filamentary structures associated with this supercluster. This indicates that the filaments would eventually evolve into separate structures.

Corona Borealis supercluster. The Corona Borealis supercluster (SCL158 in Einasto et al. 2001) is a prominent example of a supercluster in the northern sky. This structure comprises $\simeq$500 galaxies at $z = 0.07$, with a nearly spherical morphology. We find that Corona Borealis is part of a larger FVS, which also includes the superclusters SCL805 and SCL761 identified by Einasto et al. (2006). According to our analysis, since the total luminosity of this FVS is well beyond the threshold luminosity calibrated using the simulation, these structures are candidates to merge and form a single virialized system in the future.

Bootes superclusters. The Bootes supercluster (SCL138 in Einasto et al. 2001) is located at $z \simeq 0.065$ and Bootes-A (SCL150) lies directly behind at $z \simeq 0.11$. These superclusters have not been widely studied. We find that a single FVS of filamentary shape can be associated with each one of these superclusters.

The comparison presented in this section helps visualize the differences that can be found between different superstructure catalogues; our approach has the relative advantage of allowing an interpretation of known structures in terms of whether they will evolve in the future into single virialized structures. However, we remind the reader that this interpretation depends on the assumed cosmology, which in the present case is the concordance ΛCDM model, as well as on the different hypotheses adopted.

6 CLUSTERS AND GROUPS WITHIN FVSs

Although it has been claimed that the clustering properties of dark matter haloes depend exclusively on their total mass, recent analyses of numerical simulations have shown that they can be strongly affected by their assembly history (see e.g. Lacerna & Padilla 2011, and references therein). If galaxy groups and clusters within superstructures have undergone a different evolution, then systematic differences are to be expected at present. The following analysis could help to address the role of the large-scale structure in the formation and evolution of galaxies. In this section, we derive a simple statistical analysis concerning groups of galaxies and the FVS. To this end, we use three different samples of galaxy systems: (i) groups of galaxies identified in the SDSS-DR7 (see Section 2), suitable to search for correlations between the halo mass and the large-scale environment they inhabit; (ii) Abell-ACO cluster catalogue (Andernach 1991) that provides redshift measurements of 1059 clusters in the footprint area of the SDSS-DR7; and (iii) X-ray clusters of galaxies, from the RASS catalogue (Popesso et al. 2004) providing a suitable sample of bright X-ray clusters within the SDSS area.

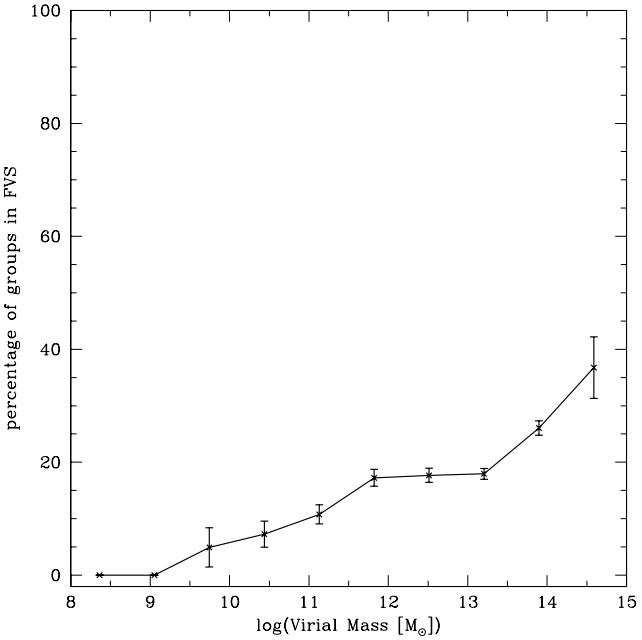

Figure 9. Percentage of DR7 galaxy groups inside FVSs with respect to the total number of groups into virial mass bins. The first and second mass bins comprise 21 galaxy groups, although none of them is located into a FVS.

We have computed the fraction of galaxy groups/clusters within FVSs as a function of their mass (Fig. 9). In this figure, error bars indicate Poisson uncertainties given by

$$\sigma\left(M_{\rm vir}^{(i)}\right) = \sqrt{N_{\rm in\,FVSs}^{(i)}}\Big/ N_{\rm all}^{(i)}, \qquad (7)$$

where $N_{\rm in\,FVS}^{(i)}$ is the number of groups/clusters inside a FVS in the ith mass bin and $N_{\rm all}^{(i)}$ is the total number of groups in the same mass bin. As can be appreciated, the fraction of groups within FVSs is greater for higher group masses. This result is also present in the catalogue of Abell-ACO clusters. This catalogue supplies 177 clusters within the coverage area of the SDSS-DR7, out of which 119 lie within the supercluster sample defined by Einasto et al. (2001) and 63 lie within FVSs. A total number of 55 Abell clusters are found in both catalogues. We compute the fraction of Abell clusters within FVSs as a function of the richness class parameter. We find only 14.5 per cent of type 0 clusters within FVSs, a value that increases for richer Abell clusters: 24.4 per cent for type 1, 34.4 per cent for type 2 and 41.7 per cent for type 3 clusters. Thus, there is a significantly larger probability of the richest Abell clusters to be in FVSs, in contrast to poor clusters.

It is also worth studying X-ray-emitting clusters of galaxies. While Abell clusters have an estimate of their richness that is discrete and approximate, the X-ray cluster catalogue provides X-ray luminosities, known to be good indicators of the underlying gravitational potential well (Rykoff et al. 2008). The catalogue of X-ray clusters also allows to study the fraction of clusters inside FVSs as a function of the X-ray luminosity. We obtain the same trend in this fraction as in the case of DR7 groups, as it can be seen from Fig. 10. However, while the fraction of systems inside FVSs is at most 0.3 for the DR7 groups (except for the last virial mass bin, which has a large uncertainty), we find that 85 per cent of the clusters with $L_{\rm X} > 4\,10^{37}$ W are part of a FVS. A similar value is found for superclusters by Einasto et al. (2001) using a compilation of X-ray

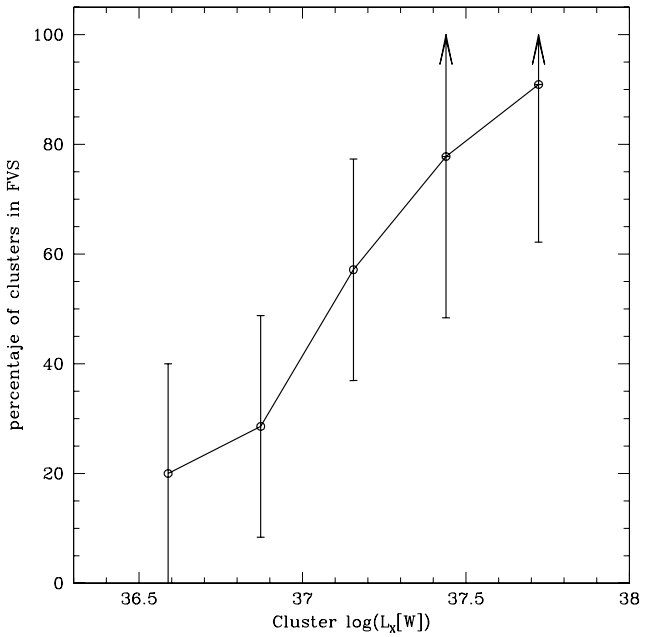

Figure 10. Percentage of X-ray clusters in FVSs with respect to the total number of X-ray clusters, as a function of the X-ray luminosity.

clusters based on the RASS. The authors also found that in rich and very rich superclusters the fraction of X-ray clusters is higher than the fraction of Abell clusters, consistent with our findings.

The results of this section are in agreement with the expectation of an assembly bias scenario, where the oldest, most massive systems are preferentially located in present-day overdense regions. Also, this suggests that the most frequent future cluster merger events will be associated with the most massive clusters within FVSs.

7 DISCUSSION

On the observational side, catalogues of superstructures have been presented on increasingly larger galaxy data sets (see Liivamägi et al. 2010, and references therein). These catalogues provide important characterizations of the largest scale structures and allow for different tests of structure formation models. Regarding the evolution of these structures, numerical simulations reveal the conditions by which these systems would evolve into isolation and dynamical equilibrium within the ΛCDM scenario. Busha et al. (2005) consider the long-term evolution of large structures, up to $a = 100$, using numerical simulations, and analyse the definition of a radius that encloses all the mass that ultimately will form an isolated structure. The authors find that a transition region is prevalent during the matter-dominated era ($a < a_{\rm eq}$), between an inner hydrostatic region and an outer region that expands with the perturbed Hubble flow. In this intermediate region, the accretion of matter towards the mass concentration is complex and gives rise to a variety of definitions of scales to describe clusters. At later times, the accretion region narrows and the hydrostatic and turnaround scales merge to form a single zero-velocity surface that unambiguously defines the halo mass. Araya-Melo et al. (2009) argue that, once Λ has started to dominate the expansion of the universe, the cosmic web growth stops, so that the spatial distribution of superclusters is essentially the same starting from the present epoch. The authors identify superclusters on the basis of criteria presented in Dünner et al. (2006). These criteria, based on the spherical collapse model and implemented on N-body simulations, allow to develop a method to isolate structures in the present universe in redshift space that will eventually form a bound structure. In a subsequent work, Dünner et al. (2007) presents a detailed method to be applied in observational data. This method is based on the assumption of spherical collapse and makes use of projected velocity envelope templates and mass profiles.

The 'gravitationally bound' criterion is widely used and was also applied to our nearby Universe. Nagamine & Loeb (2003) performed a numerical simulation with initial conditions at $z = 0$ reproducing the observed galaxy distribution in the local Universe. They conclude that the mass overdensity of the Local Group is above the required threshold to be a bound structure in the future. According to the authors, Andromeda and the Milky Way will probably merge, while our Local Group and the Virgo cluster will not form a virialized structure in the future.

From a theoretical point of view, Einasto et al. (2010b) decompose the luminosity density field of Liivamägi et al. (2010) using a wavelet analysis. They also study the formation of the cosmic web based on the evolution of the density perturbation phases in numerical simulations. They state that very rich superclusters are the result of large-scale ($\lambda \geq 32\,h^{-1}$ Mpc) density waves, combined in similar phases. Also, the cosmic web develops in early stages of the Universe evolution, and it is generated by the phase synchronization.

The largest supercluster catalogue constructed so far with SDSS-DR7 data (Liivamägi et al. 2010) allows to test our procedure and compare the results. As they apply the density field method using a wide range of threshold density parameters (analogues to our $D_{\rm T}$), we can directly contrast the final results of both catalogues for the same value of $D_{\rm T} = 5.5$. The Liivamägi et al. (2010) catalogue is deeper, so we restrict the analysis to $z = 0.12$, the limit of our main sample of FVSs. Up to this distance, we identify 150 FVSs compared to 142 superclusters in the Liivamägi et al. (2010) catalogue. In the upper panel of Fig. 11, we show the luminosity and volume of these structures. From the available list of galaxies in superclusters of Liivamägi et al. (2010), we selected a subsample of 83.798 galaxies, with the same limits as our sample S2 ($0.04 < z < 0.12$ and $M_r < -20.47$). We find that 79.4 per cent of the galaxies in superclusters also belong to a FVS and only the 3.4 per cent of galaxies outside superclusters are associated with a FVS. We also analyse the galaxies within each supercluster separately, defining the fraction of galaxies in the supercluster that are part of a FVS, $f_{\rm IN}$, and the fraction of galaxies in the supercluster that do not belong to any FVS, $f_{\rm OUT}$.

In the lower panel of Fig. 11, we show the $f_{\rm IN}$ fraction for the galaxies within each supercluster. We find that 80 per cent of superclusters have $f_{\rm IN}$ over 0.65 and $f_{\rm OUT}$ lower than 0.35. The previous analyses indicate that the general features of the structures of Liivamägi et al. (2010) and those of FVSs show a very good agreement.

8 CONCLUSIONS

The properties of the largest structures in the Universe provide important information on the cosmological model. In this work, we have developed a physically motivated procedure to isolate structures in the nearby universe that will evolve into gravitationally virialized systems in the future, within a ΛCDM framework. The method starts from a smoothed luminosity density map, where high density peaks are separated as superstructure candidates. This method depends on a number of free parameters that we determined

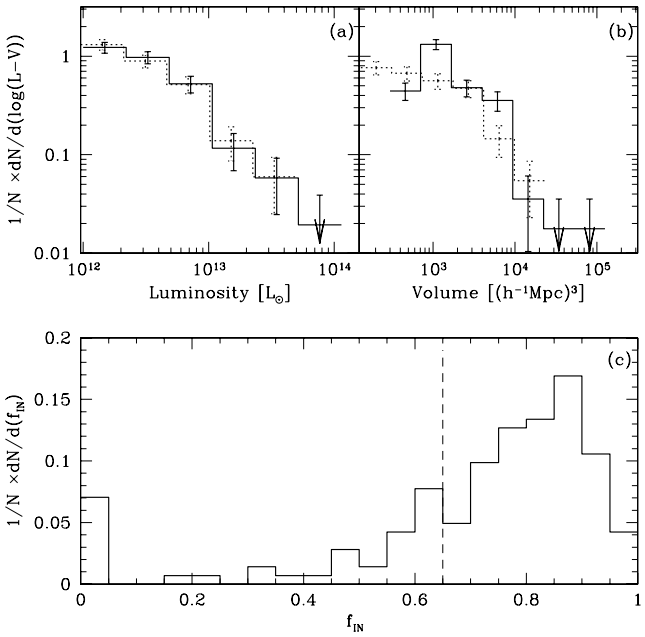

Figure 11. Upper panel: luminosity (a) and volume (b) for FVSs obtained from sample S2 (solid line) and for superclusters in the catalogue of Liivamägi et al. (2010) (dotted line). Error bars are Poisson uncertainties within each bin. Lower panel: fraction of galaxies in superclusters that also belong to a FVS, $f_{\rm IN}$. 80 per cent of superclusters have at least 65 per cent of their galaxies within FVSs, represented by the vertical dashed line.

on a theoretical basis. We adopted an Epanechnikov kernel following recent similar implementations of the method (e.g. Einasto et al. 2007b; Costa-Duarte et al. 2011). We then calibrated the luminosity overdensity parameter $D_{\rm T}$ according to results from Dünner et al. (2006) who used numerical simulations to establish the conditions for a superstructure to be virialized at $a \sim 100$. We find that a cut in the total luminosity of superstructures at $L = 10^{12}\,{\rm L}_{\odot}$ is convenient to additionally clean the sample of FVSs (see Fig. 2). This is due to the fact that although some superstructures have a total luminosity overdensity above the critical value, their mass can still be not enough to ensure the future collapse on to a virialized system. We used a mock catalogue to further constrain and test the reliability of the identification method. We defined three samples of FVSs from volume-limited samples of galaxies. From the comparison of these samples, we conclude that the method is not affected by the constraints in the survey redshift and the luminosity of galaxies, since the small differences can be explained by the corrections implemented, assuming a universal luminosity function.

The joint analysis of group catalogues and the samples of FVSs indicates that the fraction of groups within FVSs increases with the virial mass (see Fig. 9). The fraction of X-ray clusters belonging to FVSs is significantly larger and also increases with the X-ray luminosity (Fig. 10). This is consistent with the assembly bias scenario, with massive, old assembled systems located preferentially in present-day superstructures as FVSs. Thus, future cluster merger events will often involve the most massive, bright X-ray clusters. We have also analysed particular superclusters previously studied by other authors. Many known superclusters are found to be coincident with one or more FVSs in our sample. As an example, our analysis shows that the Ursa Major supercluster is composed of four filaments, each having a distinct FVS, and the Corona Borealis and Bootes superclusters are clearly associated with FVSs in our catalogue.

ACKNOWLEDGMENTS

We thank the referee, Jaan Einasto, for his thorough review and highly appreciate the comments and suggestions, which greatly improved this work. This work was partially supported by the Consejo Nacional de Investigaciones Científicas y Técnicas (CONICET) and the Secretaría de Ciencia y Tecnología, Universidad Nacional de Córdoba, Argentina. Funding for the SDSS and SDSS-II has been provided by the Alfred P. Sloan Foundation, the Participating Institutions, the National Science Foundation, the US Department of Energy, the National Aeronautics and Space Administration, the Japanese Monbukagakusho, the Max Planck Society and the Higher Education Funding Council for England. The SDSS website is http://www.sdss.org/. The SDSS is managed by the Astrophysical Research Consortium for the Participating Institutions. The Royal Astronomical Society Participating Institutions are the American Museum of Natural History, Astrophysical Institute Potsdam, University of Basel, University of Cambridge, Case Western Reserve University, University of Chicago, Drexel University, Fermilab, the Institute for Advanced Study, the Japan Participation Group, Johns Hopkins University, the Joint Institute for Nuclear Astrophysics, the Kavli Institute for Particle Astrophysics and Cosmology, the Korean Scientist Group, the Chinese Academy of Sciences (LAMOST), Los Alamos National Laboratory, the Max-Planck-Institute for Astronomy (MPIA), the Max-Planck-Institute for Astrophysics (MPA), New Mexico State University, Ohio State University, University of Pittsburgh, University of Portsmouth, Princeton University, the United States Naval Observatory and the University of Washington. The Millennium Run simulation used in this paper was carried out by the Virgo Supercomputing Consortium at the Computer Centre of the Max Planck Society in Garching. The semi-analytic galaxy catalogue is publicly available at http://www.mpa-garching.mpg.de/galform/agnpaper.

REFERENCES

Abazajian K. N. et al., 2009, ApJS, 182, 543
Andernach H., 1991, in Colless M. M., Babul A., Edge A. C., Johnstone R. M., Raychaudhury S., eds, Clusters and Superclusters of Galaxies. Institute of Astronomy, Cambridge, p. 65
Araya-Melo P. A., Reisenegger A., Meza A., van de Weygaert R., Dünner R., Quintana H., 2009, MNRAS, 399, 97
Basilakos S., Plionis M., Rowan-Robinson M., 2001, MNRAS, 323, 47
Baugh C. M. et al., 2004, MNRAS, 351, L44
Blanton M. R. et al., 2003a, AJ, 125, 2348
Blanton M. R. et al., 2003b, ApJ, 592, 819
Bower R. G., McCarthy I. G., Benson A. J., 2008, MNRAS, 390, 1399
Broadhurst T. J., Ellis R. S., Koo D. C., Szalay A. S., 1990, Nat, 343, 726
Busha M. T., Evrard A. E., Adams F. C., Wechsler R. H., 2005, MNRAS, 363, L11
Colless M. et al., 2001, MNRAS, 328, 1039
Costa-Duarte M. V., Sodré L., Jr, Durret F., 2011, MNRAS, 411, 1716
Dolag K., Hansen F. K., Roncarelli M., Moscardini L., 2005, MNRAS, 363, 29
Dünner R., Araya P. A., Meza A., Reisenegger A., 2006, MNRAS, 366, 803
Dünner R., Reisenegger A., Meza A., Araya P. A., Quintana H., 2007, MNRAS, 376, 1577
Einasto J., Saar E., Klypin A. A., 1986, MNRAS, 219, 457
Einasto M., Einasto J., Tago E., Dalton G. B., Andernach H., 1994, MNRAS, 269, 301
Einasto M., Tago E., Jaaniste J., Einasto J., Andernach H., 1997, A&AS, 123, 119
Einasto M., Einasto J., Tago E., Müller V., Andernach H., 2001, AJ, 122, 2222
Einasto J. et al., 2006, A&A, 459, L1

Einasto J. et al., 2007a, A&A, 462, 397
Einasto J. et al., 2007b, A&A, 462, 811
Einasto M. et al., 2007c, A&A, 476, 697
Einasto M. et al., 2010a, A&A, 522, A92
Einasto J. et al., 2010b, preprint (arXiv:1012.3550)
Flores-Cacho I. et al., 2009, MNRAS, 400, 1868
Frisch P., Einasto J., Einasto M., Freudling W., Fricke K. J., Gramann M., Saar V., Toomet O., 1995, A&A, 296, 611
Génova-Santos R., Rubiño-Martín J. A., Rebolo R., Battye R. A., Blanco F., Davies R. D., 2008, MNRAS, 391, 1127
Génova-Santos R., Padilla Torres C. P., Rubiño Martín J. A., Gutiérrez C. M., Rebolo R., 2010, MNRAS, 403, 1531
González R. E., Padilla N. D., 2010, MNRAS, 407, 1449
Górski K. M., Hivon E., Banday A. J., Wandelt B. D., Hansen F. K., Reinecke M., Bartelmann M., 2005, ApJ, 622, 759
Granett B., Neyrinck M., Szapudi I., 2009, BAAS, 41, 284
Icke V., 1984, MNRAS, 206, 1P
Kopylova F. G., Kopylov A. I., 2006, Astron. Lett., 32, 84
Lacerna I., Padilla N., 2011, MNRAS, 412, 1283
Liivamägi L. J., Tempel E., Saar E., 2010, preprint (arXiv:1012.1989)
Merchán M. E., Zandivarez A., 2005, ApJ, 630, 759
Murphy D. N. A., Eke V. R., Frenk C. S., 2011, MNRAS, 413, 2288
Nagamine K., Loeb A., 2003, New Astron., 8, 439
Park D., Lee J., 2007, ApJ, 665, 96
Paz D. J., Lambas D. G., Padilla N., Merchán M., 2006, MNRAS, 366, 1503
Peacock J. A. et al., 2001, Nat, 410, 169
Penton S. V., Stocke J. T., Shull J. M., 2002, ApJ, 565, 720
Platen E., van de Weygaert R., Jones B. J. T., 2008, MNRAS, 387, 128
Popesso P., Böhringer H., Brinkmann J., Voges W., York D. G., 2004, A&A, 423, 449
Porter S. C., Raychaudhury S., Pimbblet K. A., Drinkwater M. J., 2008, MNRAS, 388, 1152
Rykoff E. S. et al., 2008, MNRAS, 387, L28
Shandarin S. F., Sheth J. V., Sahni V., 2004, MNRAS, 353, 162
Shane C. D., 1956, Vistas Astron., 2, 1574
Shane C. D., Wirtanen C. A., 1954, AJ, 59, 285
Shapley H., 1961, J. R. Astron. Soc. Can., 55, 273
Shapley H., Ames A., 1930, Harv. Coll. Obs. Bull., 880, 1
Shectman S. A., Landy S. D., Oemler A., Tucker D. L., Lin H., Kirshner R. P., Schechter P. L., 1996, ApJ, 470, 172
Springel V. et al., 2005, Nat, 435, 629
Stocke J. T., Shull J. M., Penton S., Donahue M., Carilli C., 1995, ApJ, 451, 24
Stoughton C., Lupton R. H., Bernardi M., Blanton M. R., Burles S., Castander F. J., Connolly A. J., Eisenstein D. J., 2002, AJ, 123, 485
Strauss M. A., Weinberg D. H., Lupton R. H., Narayanan V. K., Annis J., Bernardi M., Blanton M., Burles S., 2002, AJ, 124, 1810
Wray J. J., Bahcall N. A., Bode P., Boettiger C., Hopkins P. F., 2006, ApJ, 652, 907
Zapata T., Perez J., Padilla N., Tissera P., 2009, MNRAS, 394, 2229
Zucca E., Zamorani G., Scaramella R., Vettolani G., 1993, ApJ, 407, 470

This paper has been typeset from a TEX/LATEX file prepared by the author.